ARTICLES
PUBLISHED ONLINE: 27 SEPTEMBER 2009 | DOI: 10.1038/NGEO636

nature geoscience

Slip maxima at fault junctions and rupturing of barriers during the 2008 Wenchuan earthquake

Zheng-Kang Shen[1,2,3]★, Jianbao Sun[1], Peizhen Zhang[1], Yongge Wan[4], Min Wang[1], Roland Bürgmann[5], Yuehua Zeng[6], Weijun Gan[1], Hua Liao[7] and Qingliang Wang[8]

The disastrous 12 May 2008 Wenchuan earthquake in China took the local population as well as scientists by surprise. Although the Longmen Shan fault zone—which includes the fault segments along which this earthquake nucleated—was well known, geologic and geodetic data indicate relatively low (<3 mm yr^{-1}) deformation rates. Here we invert Global Positioning System and Interferometric Synthetic Aperture Radar data to infer fault geometry and slip distribution associated with the earthquake. Our analysis shows that the geometry of the fault changes along its length: in the southwest, the fault plane dips moderately to the northwest but becomes nearly vertical in the northeast. Associated with this is a change in the motion along the fault from predominantly thrusting to strike-slip. Peak slip along the fault occurs at the intersections of fault segments located near the towns of Yingxiu, Beichuan and Nanba, where fatalities and damage were concentrated. We suggest that these locations represent barriers that failed in a single event, enabling the rupture to cascade through several fault segments and cause a major moment magnitude (M_w) 7.9 earthquake. Using coseismic slip distribution and geodetic and geological slip rates, we estimate that the failure of barriers and rupture along multiple segments takes place approximately once in 4,000 years.

The 12 May 2008 Wenchuan earthquake was the largest seismic event in China in more than 50 years. It devastated cities along the northwest margin of the Sichuan basin (Fig. 1), causing fatalities of more than 80,000 (ref. 1). The earthquake occurred on the Longmen Shan fault zone, which is predominantly a convergent zone with a dextral component, separating the Sichuan basin from the eastern margin of the Tibetan plateau[2]. Three major subparallel faults have been mapped to constitute the northeast trending Longmen Shan fault zone: the Pengguan fault (PGF) is to the east along the mountain front, about 10–15 km to its west lies the Beichuan fault (BCF) and the Wenchuan–Maowen fault lies about another 30 km west of the BCF (Fig. 1; ref. 3). All of the faults are northwest dipping, with the BCF and PGF converging into the same ramp system in the mid-crust[2–5]. Field geological studies found evidence of Holocene activity at least for the central PGF and BCF (refs 6–9). The geological-fault slip-rate estimates, however, are fairly low, about 0.3–0.6 mm yr^{-1} of reverse and ~1.0 mm yr^{-1} dextral faulting for the BCF, and 0.2 mm yr^{-1} reverse faulting for the PGF, averaged over the past ~10,000 years (ref. 10). Such low slip rates are consistent with Global Positioning System (GPS) estimates of the shortening rate across the Longmen Shan range of <3 mm yr^{-1} (refs 11, 12) or 1.5±1.0 mm yr^{-1} (ref. 13).

Seismological studies indicate that the Wenchuan mainshock started on the BCF about 30 km southwest of Yingxiu, and propagated unilaterally northeastward[14]. Surface breaks are found along both the BCF and PGF (refs 3, 15–17). The BCF branches into two segments east of Yingxiu, where the primary segment strikes southwestward and the other strand strikes westward through Yingxiu (Fig. 1). Both segments ruptured during the earthquake, and the largest surface slip of ~6.2 m vertical and ~4.5 m dextral motion is found along a ~20 km stretch of the fault northeast of the branching point[3]. There were no mapped fault surface breaks for ~7 km northeast of this 20 km stretch, beyond which rupture was observed along two conjugate segments, one along the primary BCF trending northeast, and the other (the Xiaoyudong segment) trending southeast and connecting to the PGF (Fig. 1). Another peak of coseismic surface offsets on the BCF is found near Beichuan, with 6.5 m vertical and 2.5 m dextral motion, respectively[3]. It is located at a fault juncture, where the BCF bends ~25° clockwise and almost intersects with the Wenchuan–Maowen fault. Yingxiu and Beichuan suffered from the greatest fatalities (~7,700 deaths at Yingxiu with a population of about 12,000 (ref. 18), and ~5,500 deaths at Beichuan with a population of less than 20,000; ref. 19) and most severe structural damage in the earthquake. The maximum surface offset along the PGF is ~3.5 m, mainly in the vertical component[3].

The surface breaks along the BCF trace from ~20 km southwest of Yingxiu (30.95° N, 103.45° E) to ~10 km southwest of Qingchuan (32.50° N, 105. 20° N), for a total length of ~235 km (ref. 3). Aftershocks, however, extend beyond both ends of the surface rupture for another 55 and 30 km, respectively (Fig. 1). This suggests that a significant portion of the fault rupture did not break to the surface at both ends, and the rupture could be as long as ~320 km. Seismic moment released during the mainshock was measured at 7.6×10^{20} N m by the United States Geological Survey, corresponding to $M_w = 7.9$ (ref. 20). Teleseismic studies indicate unilateral propagation along a 280-km-long rupture, with two slip maxima of about 9 m at ~10 km

[1]State Key Laboratory of Earthquake Dynamics, Institute of Geology, China Earthquake Administration, PO Box 9803, Beijing 100029, China, [2]Department of Geophysics, School of Earth and Space Sciences, Peking University, Beijing 100871, China, [3]Department of Earth and Space Sciences, University of California, Los Angeles, California 90095-1567, USA, [4]College of Disaster Prevention Science and Technology, Yanjiao, Sanhe, Hebei 101601, China, [5]Department of Earth and Planetary Science, University of California, Berkeley, California 94720-4767, USA, [6]Golden Office, US Geological Survey, Colorado 80401, USA, [7]Sichuan Seismological Bureau, Chengdu 610041, China, [8]Second Monitoring Center, China Earthquake Administration, Xi'an 710054, China. *e-mail: zshen@ies.ac.cn; zshen@ucla.edu.

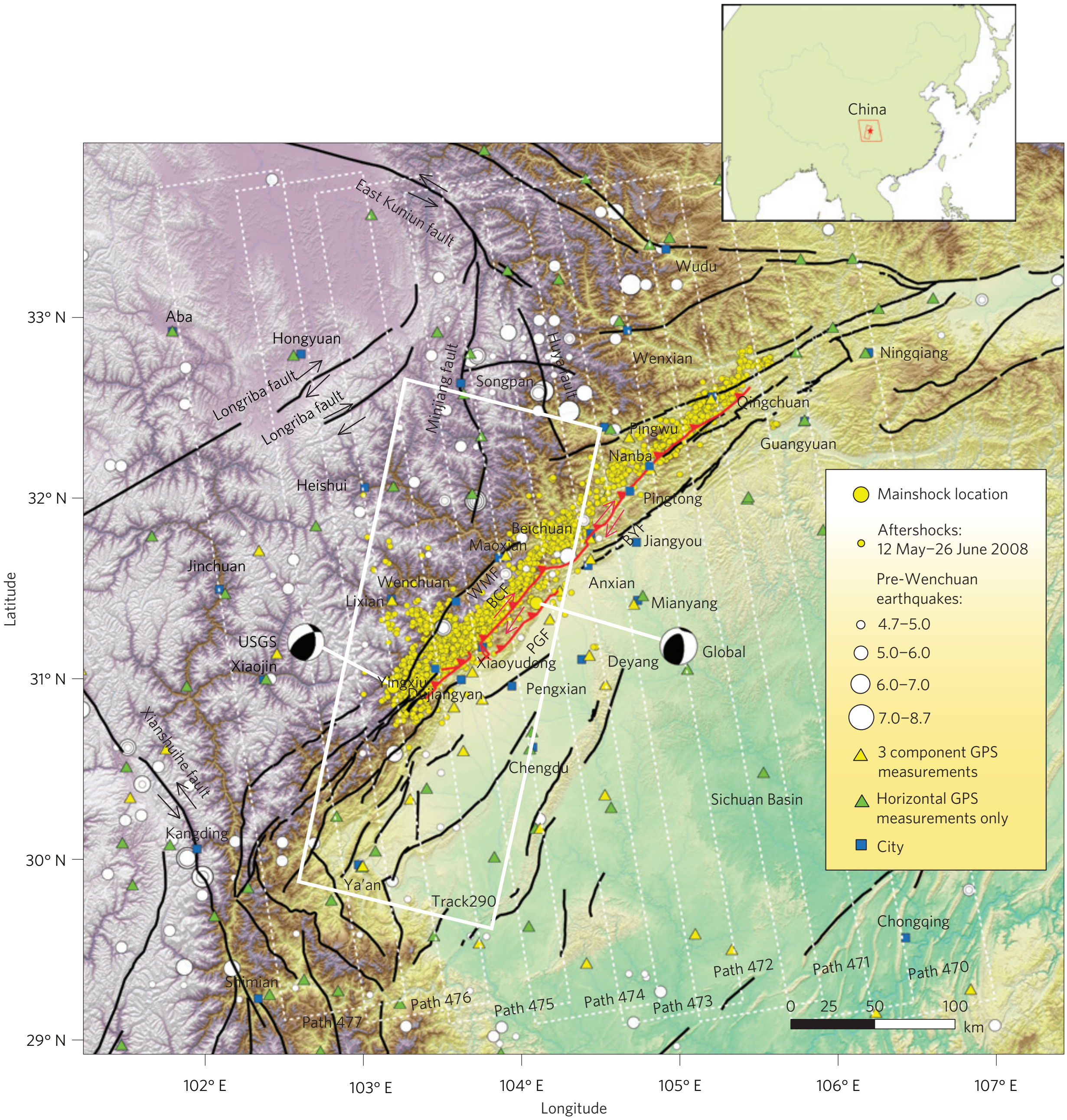

Figure 1 | Tectonic setting of the Wenchuan earthquake. The study region covered by the InSAR images is depicted in the inset map. The areas covered by ALOS (with phased-array-type L-band synthetic aperture radar (PALSAR) sensor) paths 470–477 and Envisat satellite (with Advanced Synthetic Aperture Radar (ASAR) sensor) track 290 are shown as white dashed and white solid rectangles respectively. Black and red lines indicate regional faults and surface traces of coseismic rupture[3]. Green and yellow triangles denote GPS stations whose horizontal-only and horizontal+vertical coseismic offsets are used, respectively. Two mainshock focal mechanism solutions are from United States Geological Survey and Global CMT, respectively. The white and yellow circles show $M > 4.7$ earthquakes of the past century and the Wenchuan aftershocks, respectively. WMF, Wenchuan–Maowen fault.

depth between Yingxiu and Wenchuan and between Beichuan and Pingtong, respectively[14].

Coseismic deformation observed using GPS and InSAR

In this study we use GPS data collected and processed by our group and others and Interferometric Synthetic Aperture Radar (InSAR) measurements from the Advanced Land Observation Satellite (ALOS) and Envisat satellites (see the Methods section) to constrain the geometry and slip distribution of a coseismic rupture model. Only small amounts of postseismic deformation are included in the surface displacement measurements (see the Methods section). The largest coseismic displacement observed by GPS (2.4 m west-northwestward horizontal motion and 0.68 m downward vertical motion, respectively), is measured at a site located near Beichuan on the footwall side and about 2 km from the surface rupture (Fig. 2a). Amplitudes of the displacements are reduced to ~0.1 m about 80 km from the fault. The InSAR interferograms show a total of ~0.7 m range change with L-band SAR data on either side of the fault, although missing near-field data on the hanging-wall side resulted in incomplete coverage of the total range change there. The geometry of the Wenchuan earthquake rupture on the BCF and PGF is complex. Field observations suggest that the faults have varying dip angles, with relatively shallow dip angles along the southwestern section of

NATURE GEOSCIENCE DOI: 10.1038/NGEO636

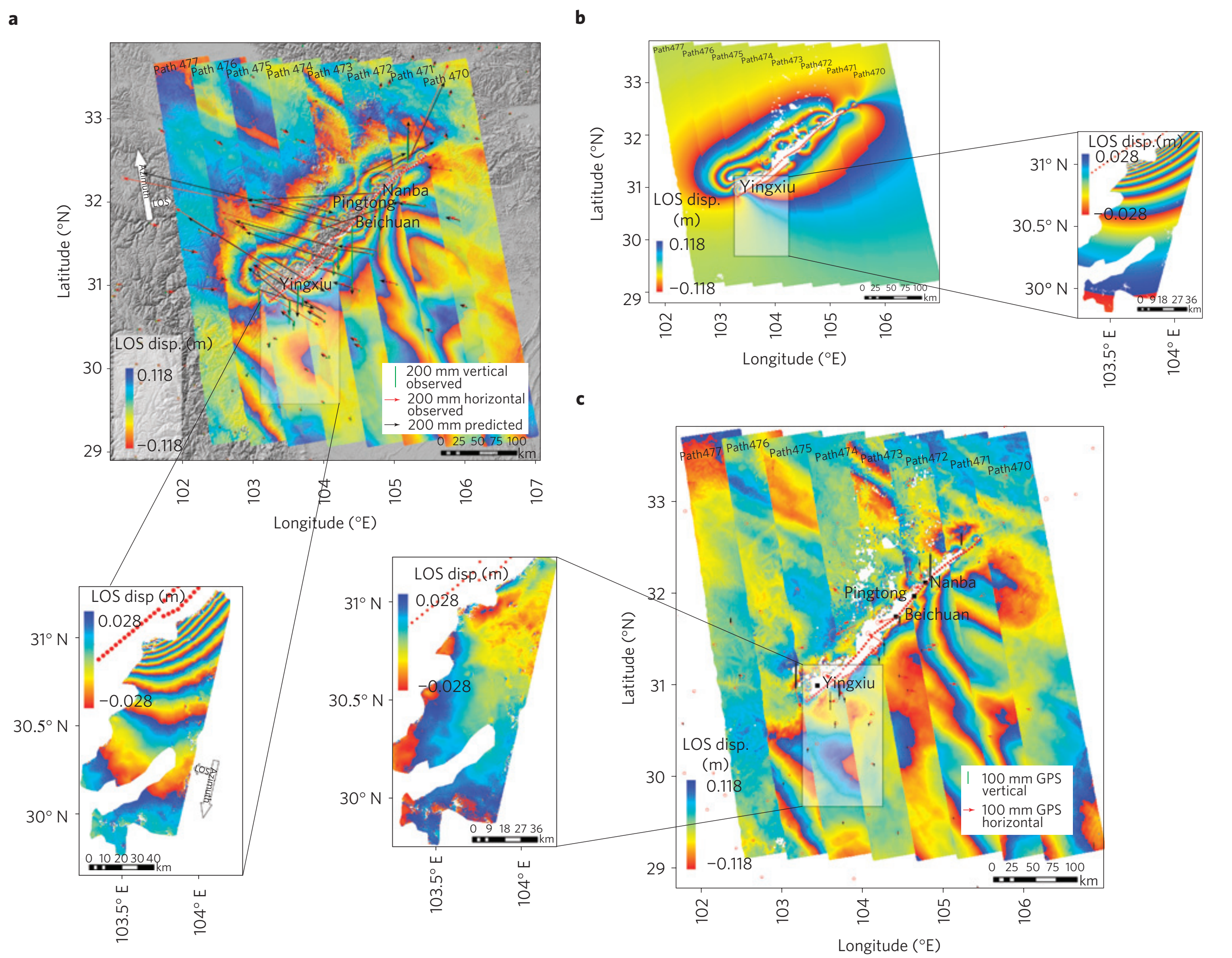

Figure 2 | InSAR and GPS data fittings. a, InSAR range-change data. The white curves depict traces of fault surface breaks, and the red dots show surface points of fault-model patches. Red arrows and green bars are GPS-observed coseismic offsets for the horizontal and vertical components. Black arrows are model-predicted coseismic offsets, horizontal or vertical. **b**, Model-predicted range changes for PALSAR and ASAR measurements. **c**, GPS and InSAR data postfit residuals. Red arrows and black columns are for the horizontal and vertical components of GPS displacements, whose uncertainties are represented as ellipses and lines at arrow and bar tips at 95% confidence.

the rupture and near vertical towards the northeastern[3]. However, dip angles measured at the surface offsets are often highly uncertain and may not reflect the dip angles at depth[3]. Precisely located aftershock hypocenters using the double-differencing method do not clearly illuminate the subsurface rupture geometry either[21]. We therefore simultaneously invert for the first-order fault geometry and the slip distribution on the fault plane in our geodetic inversion.

Fault geometry and slip distribution modelling

Our inversion finds that the BCF dips to the northwest at a moderate angle of ∼43° at the southwest end, and the fault plane gradually becomes steeper northeastward along strike, reaching ∼50° at Nanba (Fig. 3a). The dip angle jumps to ∼56° across the Nanba step-over, and increases progressively to near vertical at the northeast end of the rupture. The PGF dips shallowly at ∼28°, suggesting a common root shared with the Yingxiu–Beichuan segment of the BCF at a depth of ∼18 km, a result consistent with balanced geologic cross-sections across the southern BCF (ref. 22).

The slip distribution on the BCF shows three high-slip concentrations (Fig. 3b–d). The first one is from Yingxiu to Xiaoyudong (subsegment B10 in Fig. 3b) at 0–10 km depth. Its thrust slip averages ∼5 m, and peaks at the surface at 5.8 m. The dextral slip is also concentrated near the surface, with a maximum of about 2.5 m. A second, smaller high-slip area at 0–7 km depth near Beichuan (subsegment B6 in Fig. 3b) has comparable peak slip values, with 5.2 m and 4.8 m of thrust and dextral slip, respectively. In addition to the two prominent high-slip areas, a minor peak is located near Nanba (subsegment B4 in Fig. 3b), where the dextral and reverse slips at the surface reach local maxima of 3.0 m and 3.2 m, respectively.

The three areas of high-slip concentration are located near the intersections of fault segments. The slip maxima close to Yingxiu and Beichuan are near fault bifurcations and conjugates rupture junctions (Fig. 1), and the high slip close to Nanba spans a fault step-over, across which there is a change of fault dip angle. We therefore hypothesize that the Wenchuan earthquake broke through several high-slip junctions that connect major fault segments in a cascade rupture. These connecting structures may represent barriers that rarely fail, and would fail only when high stress has accumulated after multiple rounds of smaller events broke the adjoining individual segments. Such a cascade-rupture scenario helps explain why Yingxiu, Beichuan and Nanba experienced the highest shaking intensity of XI

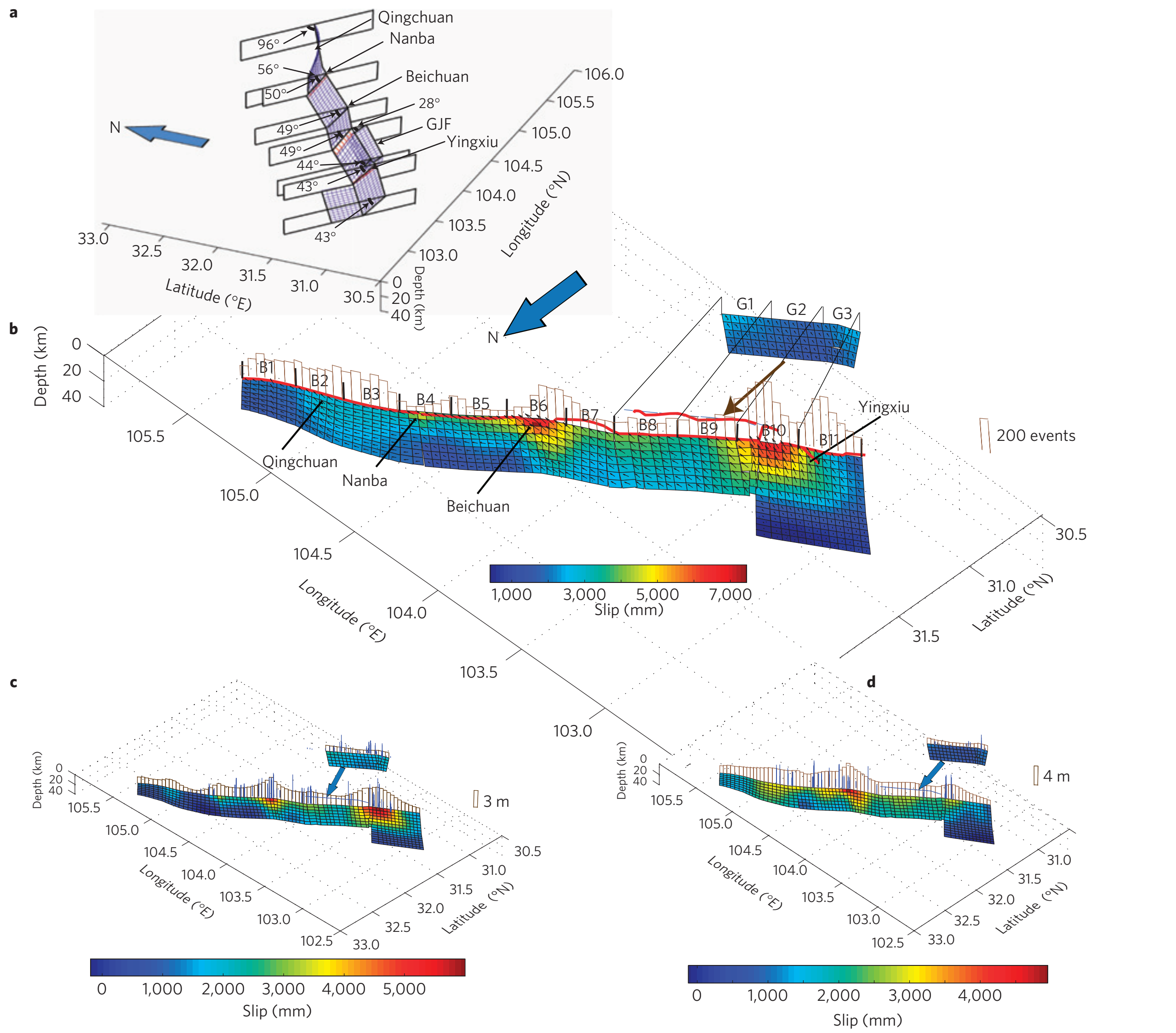

Figure 3 | Inversion results. a, Fault geometry viewed from the southwest, at 45° elevation angle. Six dip angles at fault nodal points marked with an asterisk are inverted for in the solution. **b**, Coseismic slip distribution viewed from the northwest, at 45° elevation angle. The PGF is plotted away from its actual location (whose surface trace is marked here and in **c** and **d** as a blue line). Black arrows show the slip vectors on the fault patches, whose amplitudes are denoted by the patch colour. Red lines are the mapped traces of surface breaks[3]. The brown columns show the density of aftershocks along the fault within 50 km of the surface trace. B1–B11 and G1–G3 are fault subsegments on the BCF and PGF, respectively. **c**,**d**, Reverse and dextral slip amplitudes. The brown columns denote the modelled surface offsets, in comparison with the field observations, shown as blue bars.

and suffered the greatest damage among all the towns located along the fault zone[23].

Moderate amounts of slip are detected along the PGF, with about 1.5 m and 0.7 m of average thrust and dextral motions and peak values of ~2.0 m thrust and 1.5 m dextral slip near its northeast corner close to the surface (Fig. 3). These results agree with geologically measured average surface offsets[3].

Our result also demonstrates moderate amounts of slip on the shallowly dipping fault segment extending northwestward from down-dip of the southwest segment of the BCF (subsegment B10 in Fig. 3b). Peak values of thrust motion reach ~2.0 m close to the hinge connecting to the southwest segment of the BCF. Model inversions without this deep extension produced mechanically implausible results and fit the data significantly worse (see Supplementary Note S1). We conclude that reverse faulting occurred not only on the steep part of the ramp close to the surface but also on a down-dip, near-horizontal detachment fault plane, located up to 30 km away from the surface break.

To estimate the seismic moment release of the fault rupture we integrate the thrust and dextral components along strike and down-dip assuming a shear modulus of 3×10^{10} Pa, and obtain the total seismic moment release of 8.03×10^{20} N m, equivalent to an event of M_w 7.93. This estimate, however, includes a minor contribution from postseismic deformation, because the postearthquake GPS and InSAR measurements were observed with some delays (from days to weeks). Assuming that coseismic and postseismic slips were in the upper and mid-crust respectively and separated at the depth of 20 km (suggested by the lower bound of aftershock depth range[21]), we determine the coseismic moment release above this depth as 7.30×10^{20} N m, equivalent to an event of M_w 7.91. Ongoing analysis of continuous GPS measurements during the early postseismic period[24] supports this first-order correction (see Supplementary Note S2).

The surface slip distribution of our model agrees qualitatively with the dextral (Fig. 3d) and vertical (Fig. 3c) components of field measurements. In particular, both the locations and values

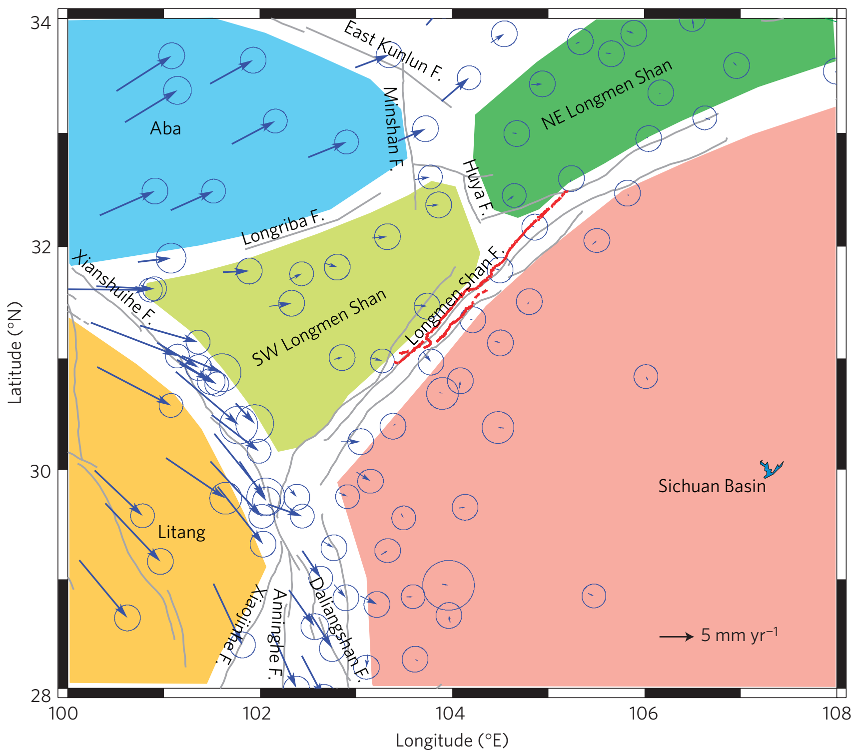

Figure 4 | Secular block-motion model. GPS velocities are referenced to the Sichuan Basin (that is, also the south China block). Error ellipses represent 70% confidence. Coloured regions denote block domains, within which the GPS site velocities are used to define the block motions. Red lines are the surface breaks of the Wenchuan earthquake[6]. Regional faults (grey lines) are modified from ref. 28.

of the peaks of vertical motions match the surface rupture offsets measured by field geologists[3]. Our slip distribution also agrees qualitatively with those derived using teleseismic data[14,25], with twin peaks of slip near Yingxiu and Beichuan. Solutions of Ji and Hayes[14], Wang *et al.*[25], and Zhang *et al.*[26] yielded larger maximum slip, ~9 m, ~12 m, and ~7 m respectively, than ours of 5–6 m, but lie at ~10–20 km depth. The difference may be due to stronger smoothing used in our model and limited depth resolution in the teleseismic studies. A recent slip-distribution model constrained using ALOS InSAR data[27], however, offered similar peak-slip locations to ours, although further details of the slip distributions are different owing to differences in data, fault geometry and smoothing constraints.

The two peaks of fault slip on subsegments B6 and B10 coincide with the locations of dense aftershock populations, suggesting strong local stress concentrations and slip on nearby faults triggered by the large coseismic slip (Fig. 3b). High aftershock concentrations on subsegments B2 and B3 in Fig. 3b between Nanba and Qingchuan coincide with moderate amounts of broadly distributed slip from the surface down to ~20 km depth. The aftershock density is considerably lower along the fault segment between Beichuan and Nanba (subsegment B5 and south part of subsegment B4) than along the neighbouring segments to the northeast and southwest, and the fault slip seems concentrated at shallow depths of less than 8 km, leaving a slip gap on the deeper part of the fault.

Regional block motion and earthquake recurrence interval

What causes the change of faulting mechanism from predominantly thrust in the southwest to dextral in the northeast? To examine how strain is partitioned in the region we devise a block-motion model constrained using regional pre-earthquake GPS velocities (Fig. 4). Our result suggests that, for the region between the East Kunlun fault to the north and the Xianshuihe fault to the south, deformation is partitioned into $4.4 \pm 0.8\,\mathrm{mm\,yr^{-1}}$ dextral slip across the Longriba fault, $1.4 \pm 0.6\,\mathrm{mm\,yr^{-1}}$ convergence and $1.7 \pm 0.6\,\mathrm{mm\,yr^{-1}}$ dextral slip across the central section of the Longmen Shan fault and $1.0 \pm 0.8\,\mathrm{mm\,yr^{-1}}$ convergence across the Minjiang–Huya fault system. Deformation across the northeast section of the Longmen Shan fault is rather minor, mainly in the form of dextral slip ($0.8 \pm 0.6\,\mathrm{mm\,yr^{-1}}$) instead of normal convergence ($0.3 \pm 0.6\,\mathrm{mm\,yr^{-1}}$). Our kinematic model is consistent with the regional topography, which shows sharp contrasts across the southwest-central Longmen Shan fault zone and the Minjiang–Huya fault system, whereas a gentler gradient is found across the northeast section of the Longmen Shan[2] (Fig. 1). More discussions about the regional tectonics and implications of our results can be found in Supplementary Note S3.

We use our results of coseismic slip and secular deformation rates to estimate earthquake recurrence intervals for individual segments of the Longmen Shan fault. We divide the BCF and PGF into 11 and three subsegments, respectively, as shown in Fig. 3b. The faults are assumed to be listric at depth, such that the fault slips interseismically across a flat fault plane at its down-dip continuation, at a rate close to the GPS-measured far-field relative motion. The coseismic slip at the surface, therefore, would be equivalent to the slip deficit accumulated interseismically at the down-dip slip rate. We first take averages within each subsegment of the strike-slip and dip-slip components of coseismic slip over the top five rows of patches, representing the seismogenic part of the crust. We then use the two slip components to obtain the amplitude of the mean coseismic slip within each subsegment.

For each fault subsegment the earthquake recurrence interval T can be estimated as $T = S/V$, where S is the mean coseismic slip on the fault subsegment and V is the secular fault slip (or slip deficit) rate. We use our coseismic slip and both the interseismic block model results and geologic slip rates of individual faults[10] to estimate earthquake recurrence intervals on individual fault subsegments. Results are listed in Table 1. The GPS-derived fault

Table 1 | Earthquake recurrence intervals of fault subsegments.

No.	Fault subsegment area	Coseismic dextral slip	Coseismic reverse slip	Coseismic slip amplitude	Secular dextral rate (GPS, Geol)	Secular reverse rate (GPS, Geol)	Secular rate (GPS, Geol)	Recurrence time (GPS, Geol)
	km^2	m	m	m	mm yr^{-1}	mm yr^{-1}	mm yr^{-1}	10^3 years
BCF 1	400	1.6	1.0	1.9	0.8, /	0.3, /	0.8, /	2.3, /
BCF 2	349	2.2	1.5	2.7	0.8, /	0.3, /	0.8, /	3.3, /
BCF 3	405	2.8	0.5	2.8	0.8, /	0.3, /	0.8, /	3.5, /
BCF 4	399	2.2	1.7	2.8	0.8, /	0.3, /	0.8, /	3.5, /
BCF 5	429	2.7	1.8	3.2	0.8, /	0.3, /	0.8, /	4.0, /
BCF 6	419	3.3	3.5	4.8	1.7, 1.0	1.4, 0.3-0.6	2.2, 1.2	2.2, 4.0
BCF 7	367	2.6	2.5	3.6	1.7, 1.0	1.4, 0.3-0.6	2.2, 1.2	1.6, 3.0
BCF 8	499	2.4	2.6	3.5	/, 1.0	/, 0.3-0.6	/, 1.2	/, 2.9
BCF 9	434	2.2	2.9	3.6	/, 1.0	/, 0.3-0.6	/, 1.2	/, 3.0
BCF 10	456	2.2	4.9	5.3	/, 1.0	/, 0.3-0.6	/, 1.2	/, 4.4
BCF 11	475	1.3	2.7	3.1	1.7, 1.0	1.4, 0.3-0.6	2.2, 1.2	1.4, 2.5
PGF 1	372	0.8	2.0	2.1	/, 0.2	/, 0	/, 0.2	/, 10.0
PGF 2	373	0.7	1.6	1.7	/, 0.2	/, 0	/, 0.2	/, 8.7
PGF 3	263	0.9	1.9	2.1	/, 0.2	/, 0	/, 0.2	/, 10.0
B8+P1	499	3.0	4.0	5.0	1.7, /	1.4, /	2.2, /	2.3, /
B9+P2	434	2.8	4.3	5.1	1.7, /	1.4, /	2.2, /	2.3, /
B10+P3	456	2.7	5.9	6.5	1.7, /	1.4, /	2.2, /	3.0, /

slip rates tend to be greater than geological estimates, because GPS results account for contributions from all of the faults in the region, whereas geological estimates account for contributions only from measured individual faults. Therefore, using GPS estimated fault slip rates tends to produce smaller estimates of recurrence interval than using geological estimates. Nevertheless our analysis yields >1,000 year recurrence intervals for all the fault segments. They are $2.3–4.0 \times 10^3$ years for the northeast section of the BCF (subsegments B1–B5) and $1.4–4.4 \times 10^3$ years for the central section of the BCF (segments B6–B11), regardless of whether the characteristic events are assumed to break the BCF only or both the BCF and PGF. The recurrence intervals on the PGF could be as large as 10^4 years. The numbers are 4.0×10^3 years and 4.4×10^3 years for the Beichuan (B6) and Yingxiu (B10) subsegments if the geological slip rate of the BCF is adopted for the estimates, suggesting the longest recurrence intervals for the two asperity subsegments on the BCF.

In conclusion, we find that the Wenchuan earthquake consecutively ruptured multiple fault segments along the BCF, as well as the subparallel PGF. Fault slip on the BCF was predominantly reverse faulting on shallowly dipping fault segments in the southwest, and changed progressively to predominantly dextral faulting on steeper fault segments as the rupture propagated northeastward. This change in geometry and slip is consistent with a southwest-to-northeast transition from more rapid and mostly convergent to slower and nearly transform motion along the Longmen Shan deduced from a block model of pre-earthquake GPS velocities. The quake produced peak slips near junctures of fault segments, suggesting that these fault junctions represent barriers that rarely fail, recurring as parts of major cascade ruptures about every 4×10^3 years. The three major high-slip junctions are near Yingxiu, Beichuan and Nanba, which suffered the highest structural damage and fatality rates among all the towns located along the fault rupture zone.

Methods

GPS and InSAR data and their processing. The GPS data are obtained by the Working Group of the Crustal Motion Observation Network of China Project[29] (with major contributions from members of our group), using data collected before and after the quake in the vicinity of the seismic region. The data are processed using the GAMIT/GLOBK (ref. 30) and QOCA (ref. 31) software. Further details about the determination of coseismic offsets and consideration of postseismic contributions to the measurements are detailed in Supplementary Notes S4 and S2.

Two kinds of SAR data are used to retrieve the coseismic signals of the Wenchuan earthquake, namely Envisat ASAR data in the C-band (5.6 cm wavelength) from ESA and ALOS PALSAR data in the L-band (23.6 cm wavelength) from JAXA. PALSAR data from eight paths (470–477) and eight frames (580–650) are processed, covering a region of ~540 km wide from west to east and ~525 km long from south to north, enclosing the entire fault rupture zone (Fig. 1, Supplementary Table S1). The epochs of postseismic PALSAR observations are within 1–7 weeks of the quake (see Supplementary Table S1), and the postseismic deformation accumulated within this time period is found to be small (a few per cent compared with the coseismic signals, see Supplementary Note S2). Details about the data processing and subsampling procedures can be found in Supplementary Note S4, and Supplementary Note S5 provides further information on how the relative weights of the GPS and InSAR data are considered in the model inversions.

Inversion of fault-rupture model. To construct the fault-rupture model we let all fault segments extend to the Earth's surface, including sections where no surface slip was observed. The surface traces of the faults are based on amplitude pixel offsets of SAR image pairs, with additional *a priori* information on fault geometry coming from distribution of aftershocks as described in Supplementary Note S6. Three sections of the fault rupture are defined in the model (Fig. 3): the main fault rupture on BCF, the secondary rupture on PGF, and a blind thrust branching westward from the down-dip end of the southwest segment of BCF. See Supplementary Method S1 for fault meshing and smoothing. We use a Newtonian nonlinear inversion procedure to solve for the fault geometry and slip distribution on faults. The fits of the coseismic slip model to the InSAR and GPS data are shown in Fig. 2. Supplementary Note S7 and Tables S2 and S3 provide further details on the fault slip model, the nonlinear inversion method and results.

Block-motion model. Our interseismic block-motion model is derived from synthesizing four epochs of campaign-mode measurements of the CMONOC project 1999–2007 (refs 32, 33). (Our results should be more precise than estimates of previous studies, because adding the 2007 epoch extends the time span of the CMONOC campaign data from 5 to 8 years compared with our previously published dataset in ref. 34). Assuming rigid blocks for the Sichuan Basin, southwest Longmen Shan, northeast Longmen Shan, Aba and Litang blocks, we estimate the angular velocity of each block with respect to the Sichuan Basin, which seems to be stable with respect to the larger South China microplate[12]. Using the block-rotation parameters we determine the relative displacement rates across the block boundaries, which provides geodetic fault slip-rate estimates and their uncertainties, taking into account all the variance/covariance among different station velocity components (Fig. 4).

Derivation of earthquake recurrence intervals on faults. For those BCF and PGF subsegments (B8–B10 and G1–G3) that are sub-parallel and ruptured together during this quake, quantification of the characteristic event's slip and the fault secular slip rate on the segment becomes less clear. If the Wenchuan earthquake is considered 'characteristic', that is, the largest events would always produce simultaneous rupture on both faults, the recurrence interval on a pair of the fault segments can then be estimated using a sum of the mean slip (weighted over the rupture areas) on the faults and the secular block motion rate relevant to the fault patch. If, however, the Wenchuan earthquake is only a rare occasion, and most of the time rupture would occur on individual faults alone, the recurrence intervals on these fault segments will then have to be estimated separately using their coseismic slips (assuming slips on both faults are 'characteristic') and secular slip rates of individual faults. Owing to limited spatial coverage of the regional GPS network, our block-motion model derived using GPS data does not have the details to differentiate individual fault slip rates from their aggregated rate. We instead use geologically estimated fault slip rates[10] to make the estimation. The corresponding uncertainties of the earthquake recurrence interval estimations are discussed in Supplementary Note S8.

Received 26 January 2009; accepted 21 August 2009; published online 27 September 2009

References

1. http://www.gov.cn/xxgk/pub/govpublic/mrlm/200805/t20080530_32846.html.
2. Burchfiel, B. C. *et al*. A geological and geophysical context for the Wenchuan earthquake of 12 May 2008, Sichuan, People's Republic of China. *GSA Today* **18,** 4–11 (2008).
3. Xu, X. *et al*. Coseismic reverse- and oblique-slip surface faulting generated by the 2008 M_w 7.9 Wenchuan earthquake, China. *Geology* **37,** 515–518 (2009).
4. Burchfiel, B. C., Chen, Z., Liu, Y. & Royden, L. H. Tectonics of the Longmen Shan and adjacent regions. *Int. Geol. Rev.* **37,** 661–735 (1995).
5. Jia, D. *et al*. Longmen Shan fold-thrust belt and its relation to the western Sichuan Basin in central China: New insights from hydrocarbon exploration. *AAPG Bull.* **90,** 1425–1447 (2006).
6. Densmore, A. L. *et al*. Active tectonics of the Beichuan and Pengguan faults at the eastern margin of the Tibetan Plateau. *Tectonics* **26,** TC4005 (2007).
7. Chen, G.-G. *et al.* Primary research of the activity segmentation of Longmenshan fault zone since late Quaternary (in Chinese). *Seismol. Geol.* **29,** 657–673 (2007).
8. Li, C., Song, F. & Ran, Y. Late Quaternary activity and age constraint of the northern Longmenshan Fault Zone (in Chinese). *Seismol. Geol.* **26,** 248–258 (2004).
9. Li, Y., Zhou, R., Densmore, A. L. & Ellis, M. A. Geomorphic evidence for the late Cenozoic strike slipping and thrusting in Longmen mountain at the eastern margin of the Tibetan plateau (in Chinese). *Quat. Res.* **26,** 40–51 (2006).
10. Ma, B. *et al.* Late Quaternary slip rate in the central part of the Longmenshan Fault Zone from terrace deformation along the Minjiang River (in Chinese). *Seismol. Geol.* **27,** 234–242 (2005).
11. Chen, Z. *et al.* Global Positioning System measurements from eastern Tibet and their implications for India/Eurasia intercontinental deformation. *J. Geophys. Res.* **105,** 16215–16227 (2000).
12. Shen, Z.-K., Lu, J., Wang, M. & Burgmann, R. Contemporary crustal deformation around southeast borderland of Tibetan plateau. *J. Geophys. Res.* **110,** B11409 (2005).
13. Wang, Y. *et al.* GPS-constrained inversion of present-day slip rates along major faults of the Sichuan-Yunnan region, China. *Sci. China Ser. D* **51,** 1267–1283 (2008).
14. Ji, C. & Hayes, G. Preliminary result of the May 12, 2008 M_w 7.9 eastern Sichuan, China earthquake, US Geol. Surv., Va.; available at <http://earthquake.usgs.gov/eqcenter/eqinthenews/2008/us2008ryan/finite_fault.php>.
15. Zhang, Z. *et al.* Co-seismic ruptures of the 12 May 2008 M_w 8.0 Wenchuan earthquake, Sichuan: EW crustal shortening on oblique, parallel thrusts along the eastern edge of Tibet. *Eos* **89,** Fall Meet. Suppl., abstr. U23B-0054 (2008).
16. Li, H. *et al.* The M_w 7.9 Wenchuan earthquake of 12 May 2008, Sichuan, China: Surface rupture and oblique right-lateral coseismic thrusting. *Eos* **89,** Fall Meet. Suppl., abstr. T33A-2033 (2008).
17. Lin, A., Ren, Z., Jia, D. & Wu, X. Co-seismic thrusting slip and shortening structures produced by the 2008 M_w 7.9 Wenchuan earthquake, China. *Eos* **89,** Fall Meet. Suppl., abstr. U23B-0055 (2008).
18. http://news.xinhuanet.com/mil/2008-05/13/content_8161323.htm.
19. http://www.nowpublic.com/world/beichuan-ruins-become-museum-and-memorial.
20. http://neic.usgs.gov/neis/eq_depot/2008/eq_080512_ryan/neic_ryan_cmt.html.
21. Chen, J.-H. *et al*. Seismotectonic study by relocation of the Wenchuan *M*s 8.0 earthquake sequence (in Chinese). *Chin. J. Geophys.* **52,** 390–397 (2009).
22. Hubbard, J. & Shaw, J. H. Uplist of the Longmen Shan and Tibetan plateau, and the 2008 Wenchuan ($M = 7.9$) earthquake. *Nature* **458,** 194–197 (2009).
23. Zhang, P. Z. *et al.* Tectonic model of the great Wenchuan earthquake of May 12, 2008, Sichuan, China. *Chin. Sci. Bull. (Chinese version)* **54,** 944–953 (2009).
24. Shen, Z.-K. *et al.* Postseismic deformation monitoring of the 2008 M_w 7.9 Wenchuan earthquake using GPS. *Eos* **89,** Fall Meet. Suppl., abstr. G33C-0710 (2008).
25. Wang, W.-M., Zhao, L.-F., Li, J. & Yao, Z.-X. Rupture process of the *M*s 8.0 Wenchuan earthquake of Sichuan, China. *Chin. J. Geophys.* **51,** 1403–1410 (2008).
26. Zhang, Y., Feng, W., Xu, L., Zhou, C. & Chen, Y. Spatio-temporal rupture process of the 2008 great Wenchuan earthquake. *Sci. China Ser. D* **52,** 145–154 (2008).
27. Hao, K. X., Si, H., Fujiwara, H. & Ozawa, T. Coseismic surface-rupture and crustal deformations of the 2008 Wenchuan earthquake M_w 7.9, China. *Geophys. Res. Lett.* **36,** L11303 (2009).
28. Deng, Q.-D. (ed.) *Active Tectonics Map of China (in Chinese)* (Seismological Press, 2007).
29. Working Group of the Crustal Motion Observation Network of China Project. Coseismic displacement field of the 2008 *M*s 8.0 Wenchuan earthquake determined by GPS (in Chinese). *Sci. China Ser. D* **38,** 1195–1206 (2008).
30. King, R. W. & Bock, Y. Documentation for the GAMIT GPS analysis software, release 10.0, Mass. Inst. Technol., Cambridge (2000).
31. Dong, D. <http://gipsy.jpl.nasa.gov/qoca>.
32. Wang, M. *et al*. Contemporary crustal deformation of the Chinese continent and tectonic block model. *Sci. China Ser. D Suppl.* **46,** 25–40 (2003).
33. Niu, Z. *et al*. Contemporary velocity field of crustal movement of Chinese mainland from Global Positioning System measurements. *Chin. Sci. Bull* **50,** 939–941 (2005).
34. Gan, W. *et al*. Present-day crustal motion within the Tibetan Plateau inferred from GPS measurements. *J. Geophys. Res.* **112,** B08416 (2007).

Acknowledgements

We thank JAXA and ESA (ESA-NRSCC Dragon project 2577), particularly M. Kawai and R. Malosti for SAR data provision, and CEA and CBSM survey crews, particularly Q. Wang, for GPS data collection. Discussions with X. Xu, C. Lasserre, R. Briggs, X. Wen, Q. Liu, C. Ji, E. Fielding, P. Bird, Y. Kagan, D. Jackson, A. Sladen, J.-P. Avouac, A. Yin and P. Molnar have been helpful. Review comments of J. Langbein are appreciated. Administrative and technical support provided by Q. Li, J. Sun, W. Tao, F. Liang, X. Gao, Y. Wang, M. Hao, K. Wang and W. Chen are appreciated. This study has been supported by research grants from MSTC (2004CB418403, LED2008A05), NSFC (40674011, 40674022), CEA (IGCEA JB-09-04, 200708002) and NSF (EAR-0609656).

Author contributions

Z.-K.S., R.B., Y.Z., P.Z., and J.S. wrote the paper. J.S. and M.W. processed InSAR and GPS data. Y.W. and Z.-K.S. carried out modelling and inversion. P.Z., W.G., H.L., and Q.W. organized GPS field surveys for data collection.

Additional information

Supplementary information accompanies this paper on www.nature.com/naturegeoscience. Reprints and permissions information is available online at http://npg.nature.com/reprintsandpermissions. Correspondence and requests for materials should be addressed to Z.-K.S.